

Adaptive mitigation of time-varying quantum noise

Samudra Dasgupta^{1,2*}, Arshag Danageozian^{3#} and Travis S. Humble^{1,2†}

¹Quantum Science Center, Oak Ridge National Laboratory, Oak Ridge, Tennessee, USA

²Bredesen Center, University of Tennessee, Knoxville, Tennessee, USA

³Hearne Institute for Theoretical Physics, Department of Physics and Astronomy,
Louisiana State University, Baton Rouge, Louisiana 70803, USA

*sdasgup3@tennessee.edu, ORCID: 0000-0002-7831-745X

#arshag.danageozian@gmail.com, ORCID: 0000-0003-0044-9951

†humblets@ornl.gov, ORCID: 0000-0002-9449-0498

Abstract—Current quantum computers suffer from non-stationary noise channels with high error rates, which undermines their reliability and reproducibility. We propose a Bayesian inference-based adaptive algorithm that can learn and mitigate quantum noise in response to changing channel conditions. Our study emphasizes the need for dynamic inference of critical channel parameters to improve program accuracy. We use the Dirichlet distribution to model the stochasticity of the Pauli channel. This allows us to perform Bayesian inference, which can improve the performance of probabilistic error cancellation (PEC) under time-varying noise. Our work demonstrates the importance of characterizing and mitigating temporal variations in quantum noise, which is crucial for developing more accurate and reliable quantum technologies. Our results show that Bayesian PEC can outperform non-adaptive approaches by a factor of 4.5x when measured using Hellinger distance from the ideal distribution.

Index Terms—Device reliability, Computational accuracy, Result reproducibility, Probabilistic error cancellation, Adaptive mitigation, Spatio-temporal non-stationarity, Time-varying quantum noise, NISQ hardware-software co-design

I. INTRODUCTION

Characterizing noise in multi-qubit quantum devices is a fundamental step towards achieving fault-tolerant quantum computation. However, there is an increasing body of evidence showcasing that physical platforms for quantum computation are subject to both spatial and temporal variations [1], [2]. Namely, different qubit locations in a given quantum device experience different noise profiles, and furthermore, the statistical characteristics of the noise vary over time. These have important implications for current and future quantum technologies, especially when quantum tasks are performed on time/length scales larger than the characteristic time/length of the noise variations. An adaptive treatment of these complications is of direct relevance to quantum computing.

Modern (classical) computers have device components with failure rates of 10^{-17} or less. Current state-of-the-art quantum computers however exhibit gate-level (e.g. CNOT) failure rates of around 10^{-2} [3]. Consequently, reliability and reproducibility of results obtained from quantum computers is a problem in modern quantum information science [4]–[9]. The problem is made worse by our experimental observation that today’s NISQ (Noisy Intermediate-Scale Quantum) [10] devices are

unstable. Also, the calibration may not be up-to-date due to device drift [11]–[13]. Also, correlations within a circuit can increase errors in one part while reducing errors in another. Thus, it is often not clear what is the right optimal operating point for the compensated circuit.

Key device characterization metrics often fluctuate with time in-between calibrations (temporal instability) and also across the chip (spatial stability). These types of time-varying noise require mitigation methods that operate between calibration periods and adapt to the evolving noise sources. The quantum noise channel in fact is a random variable that needs adaptive treatment. Using inaccurate characterization data for mitigation can impact circuit reproducibility [11].

Despite rapid developments, physical platforms for quantum computation exhibit temporal variations in noise parameters. For example, temporal noise variations in superconducting qubits are among the most well-studied in literature. The current consensus attributes the variations in the latter to the presence of certain oxides on the superconductors’ surface, modeled as fluctuating two-level systems (TLS) [1], [2]. Unlike temporal variations in noise, the effects of which are magnified by the complexity of a quantum circuit, the spatial variations are dependent on the geometry and scale of the circuit implementation.

There exists an active research area that aims at addressing the time-varying nature of quantum noise within our current technology. This includes modeling [14] and characterizing such noise sources, tracking their temporal profile [15]–[20], as well as incorporating this statistical knowledge into existing quantum architectures via novel techniques, such as “spectator systems” and feedback control [21]–[23], continuous control [24], and autonomous control [25], among many others. Similarly, many advances have also been made for spatially varying noise in quantum devices [26], its effect on the choice of circuit geometry [27], as well as the interplay with cross-talk between qubits for single and two-qubit gates [28], [29].

In this article, we provide a spatio-temporal characterization of the noise variations of a transmon based IBM quantum computer. We model the multi-qubit noise by the twirled amplitude and phase damping channels. Then, we measure

and characterize the variations in single qubit T_1 and T_2 times on various relevant time and length scales. Furthermore, we show how to infer the twirled channel parameters dynamically from the noisy binary output of the quantum circuit execution. Finally, we propose a Bayesian technique [30]–[33] to implement noisy gates using probabilistic error cancellation [34], [35] in the presence of spatio-temporal variations of the twirled channels, and show how it outperforms current noisy implementations, without taking into account the spatio-temporal dependence. Our framework could be generalized and applied to various other techniques of adaptive error correction and mitigation, thereby minimizing the effects of spatio-temporally varying noise during quantum computation.

The manuscript is organized as follows. In Section II, we review evidence for spatio-temporally varying noise in superconducting qubits. Section III describes our theoretical model, along with the quantification of the degree of non-stationarity of the noise. Section IV sets the adaptive Bayesian framework for estimating the non-stationary noise parameters, which we then use to perform probabilistic error cancellation to achieve high-fidelity qubit gates. Finally, we provide the conclusion in Section V, along with open questions and future directions.

II. STOCHASTIC FLUCTUATION IN REGISTER DECOHERENCE

Decoherence refers to any loss of unitarity in state evolution, including explicit loss of coherence, energy relaxation effects, and leakage out of the qubit state space. The traditional definition of decoherence, which describes the decay of off-diagonal terms in the density matrix, is now referred to as dephasing and considered one kind of decoherence [36]. Decoherence studies typically focus on three metrics: transverse relaxation time (T_1), longitudinal relaxation time (T_2), and dephasing time (T_ϕ).

T_1 , also known as the transverse relaxation time or relaxation time, measures the attenuation of amplitude in a quantum system. It represents the probability that an excited state $|1\rangle$ will decay to the ground state $|0\rangle$ after time t , and is modeled by the function:

$$\Pr(|1\rangle \rightarrow |0\rangle) = 1 - \exp(-t/T_1). \quad (1)$$

The decay-time probability density $f_T(t)$ can be described by the exponential function:

$$f_T(t) = T_1 \exp^{-t/T_1}, \quad (2)$$

whose mean is $\mathbb{E}(T) = T_1$.

T_2 is a measure of how long it takes for a qubit in the superposition state to decay. Specifically, it measures the decay of the off-diagonal elements of the density matrix and is modeled by an exponential decay function. Therefore, it captures the loss of synchronization between the basis states of an arbitrary quantum ensemble. There are two types of T_2 time often quoted in literature [37]:

- Ramsey dephasing time T_2^* : measures the time-scale at which a quantum register experiences dephasing effects when left to evolve freely

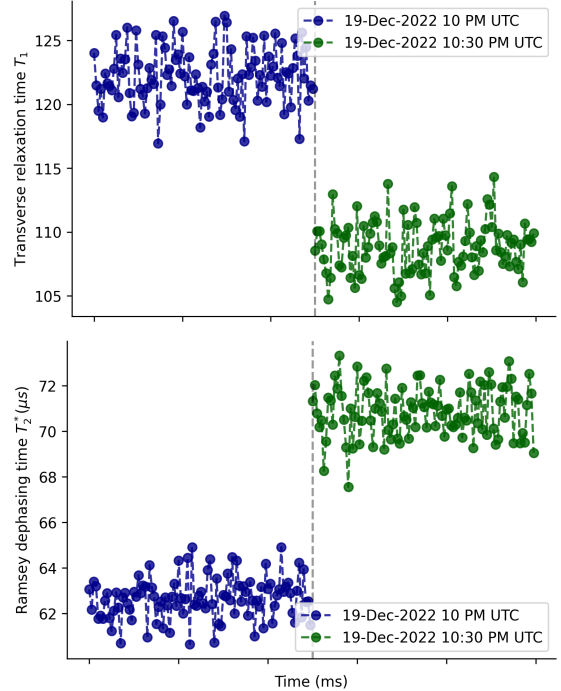


Fig. 1. This figure presents non-stationary temporal dynamics of decoherence for a qubit on IBM’s Belem device. The top figure shows T_1 relaxation time series for qubit 0, where two datasets were collected for 5 ms each on the same day, separated by a vertical line. The blue dataset varies between $116\text{--}126\mu\text{s}$ with a mean of $122\mu\text{s}$ and a standard deviation of $2\mu\text{s}$, while the green dataset varies between $104\text{--}114\mu\text{s}$ with a mean of $108\mu\text{s}$ and a standard deviation of $2\mu\text{s}$. The bottom figure displays Ramsey dephasing time (T_2) series for qubit 0, where two datasets were collected for 5 ms each on the same day, separated by a vertical line. The blue dataset varies between $67\text{--}73\mu\text{s}$ with a mean of $70\mu\text{s}$ and a standard deviation of $1\mu\text{s}$, while the green dataset varies between $60\text{--}64\mu\text{s}$ with a mean of $62\mu\text{s}$ and a standard deviation of $1\mu\text{s}$, collected around different times on the same day. The data shows significant non-stationarity in decoherence values over a 30-minute interval.

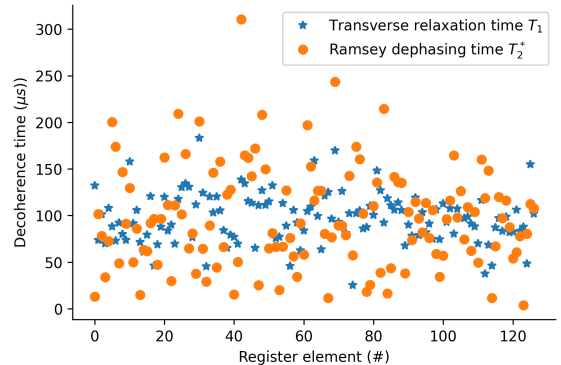


Fig. 2. This figure displays a snapshot of T_1 and T_2 times for IBM’s 127-qubit transmon device, generated from circuit execution at 14 Jan 2023 10:20 PM UTC. Each of the 127 qubits in the register is represented by a data point for T_1 and T_2 , providing a comprehensive view of the spatial variation of the decoherence times across the register.

- Hahn-echo dephasing time T_2^{echo} : uses intermediate π pulses for re-focusing to increase relaxation time.

When simulating noisy circuits, the appropriate T_2 value to use depends on whether the physical implementation of the circuit uses Hahn-echo for noise suppression or not.

Finally, the pure dephasing time (T_ϕ) is an upper bound on the decoherence time for a qubit, since thermal fluctuations in the environment inevitably cause a loss of phase coherence. However, in practice, the dominant relaxation time is usually T_2 (or sometimes T_1), rather than T_ϕ [37]. The three decoherence benchmarks are related by the Bloch-Redfield model:

$$\frac{1}{T_2} = \frac{1}{2T_1} + \frac{1}{T_\phi}. \quad (3)$$

NISQ devices display random fluctuations in decoherence times T_1 and T_2 . Therefore, the characterization often exhibits significant variability with time and register location. As shown in [38], [39], decoherence times can vary significantly from their long-term average, fluctuating by approximately 50% within an hour. The causes and mechanisms behind decoherence time fluctuations are poorly understood. In transmon registers, potential sources of fluctuations include TLS defects, quasiparticles, parasitic microwave modes, phonons, nuclear spins, paramagnetic impurities, spurious resonances, critical current noise, background charges, gate voltage fluctuations, and the electromagnetic environment [36]. Among these, TLS defects have been identified as the primary cause of decoherence [38], [40], [41]. These defects arise from deviations from crystalline order in the naturally occurring oxide layers of transmons, resulting in trapped charges, dangling bonds, tunneling atoms, or collective motion of molecules.

The fluctuations in T_1 and T_2 are exemplified by the following findings on IBM's transmon devices. On December 19, 2022, around 9:50 PM UTC, the T_1 time of qubit 0 on IBM's Belem device had a narrow variation between 17.04 μs and 17.33 μs , with a mean of 17 μs and a standard deviation of 0.05 μs . However, the T_2 time for the same qubit had a wide variation, ranging from 59 μs to 65 μs , with a mean of 62 μs and a standard deviation of 1 μs . This temporal variation at typical program execution time-scales (several hundred microseconds) is shown in Fig. 1, which shows the non-stationary temporal dynamics of coherence times in between calibration times.

When we compare the spatial variation, we find that on January 14, 2023, at 10:20 PM UTC, the T_1 time across IBM's Washington device varied widely between 25.3 μs and 183.1 μs , with a mean of 97.2 μs and a standard deviation of 26.8 μs . On the same date and time, the T_2 time for the qubits on the same device showed an even broader variation, ranging from 3.7 μs to 310.4 μs , with a mean of 97.5 μs and a standard deviation of 54.1 μs . This is shown in Fig. 2. Note that data on T_2 times for all qubits of the Washington register, after calibration on a specific day, is publicly accessible through IBM data servers and can be obtained using Qiskit. The circuits utilized by us to gather T_1 and T_2 data are depicted in Fig. 3 (a) and (b) respectively. In these circuits, the delay gates represent a 50 μs

delay, equivalent to 225,000 times the minimum time-interval achievable for such a delay circuit. To maximize qubit reuse, the software's reset and mid-circuit measurement functionalities are employed. Each estimated data used 100,000 shots.

The decoherence time fluctuations in both temporal and spatial domains can lead to inaccurate error mitigation/correction, when verifying test circuits, and unreliable quantum program output in general. Therefore, it is crucial to quantify the uncertainty of these characterizations and identify their sources and mechanisms. This will allow researchers to strike a balance between reporting reliability and precision.

III. SPATIO-TEMPORAL STOCHASTICITY OF THE PAULI NOISE CHANNEL

A. Single-qubit channel

The amplitude damping channel $\mathcal{E}^{\text{AD}}(\cdot)$ and dephasing channel $\mathcal{E}^{\text{PD}}(\cdot)$ are two fundamental sources of quantum decoherence and information loss in transmons [2], [41], [42]. A realistic model for this noise channel, denoted as APD, involves a combination of amplitude damping and dephasing.

Amplitude damping can be described by the Kraus operators E_0^{AD} and E_1^{AD} , while phase damping can be described by E_0^{PD} and E_1^{PD} , as follows [42]:

$$\mathcal{E}^{\text{AD}}(\rho) = \sum_{k=0}^1 E_k^{\text{AD}} \rho E_k^{\text{AD}\dagger}, \quad (4)$$

$$E_0^{\text{AD}} = \begin{pmatrix} 1 & 0 \\ 0 & \sqrt{1-\gamma} \end{pmatrix}, \quad (5)$$

$$E_1^{\text{AD}} = \begin{pmatrix} 0 & \sqrt{\gamma} \\ 0 & 0 \end{pmatrix}, \quad (6)$$

$$\mathcal{E}^{\text{PD}}(\rho) = \sum_{k=0}^1 E_k^{\text{PD}} \rho E_k^{\text{PD}\dagger}, \quad (7)$$

$$E_0^{\text{PD}} = \begin{pmatrix} 1 & 0 \\ 0 & \sqrt{1-\lambda} \end{pmatrix}, \quad (8)$$

$$E_1^{\text{PD}} = \begin{pmatrix} 0 & 0 \\ 0 & \sqrt{\lambda} \end{pmatrix}. \quad (9)$$

Here, $\gamma = 1 - \exp(-t/T_1)$ and $\lambda = 1 - \exp(-t/T_2)$, where t is the time scale of the decoherence process. The relation between T_1 , T_ϕ , and T_2 was previously discussed in Eq. (3). The Kraus decomposition of the combined amplitude and phase damping channel $\mathcal{E}^{\text{APD}}(\cdot)$, valid for a single qubit, can be expressed as E_0^{APD} , E_1^{APD} , and E_2^{APD} .

$$\mathcal{E}^{\text{APD}}(\rho) := \mathcal{E}^{\text{PD}} \circ \mathcal{E}^{\text{AD}} = \sum_{k=0}^2 E_k^{\text{APD}} \rho E_k^{\text{APD}\dagger}, \quad (10)$$

where,

$$E_0^{\text{APD}} = E_0^{\text{PD}} E_0^{\text{AD}} = \begin{pmatrix} 1 & 0 \\ 0 & \sqrt{[1-\gamma][1-\lambda]} \end{pmatrix}, \quad (11)$$

$$E_1^{\text{APD}} = E_0^{\text{PD}} E_1^{\text{AD}} = \begin{pmatrix} 0 & \sqrt{\gamma} \\ 0 & 0 \end{pmatrix}, \quad (12)$$

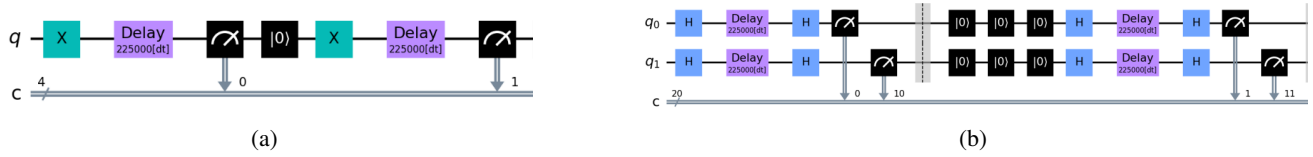


Fig. 3. We utilized the depicted circuits to gather (a) T_1 and (b) T_2 data, on Dec 19, 2022 at 10pm and 10:30pm. Here the delay gates represent a $50\mu\text{s}$ delay (225,000 times the minimum time-interval for such a delay circuit), and qubit reuse is maximized through the software's reset and mid-circuit measurement functionalities, with each estimated data utilizing 100,000 shots.

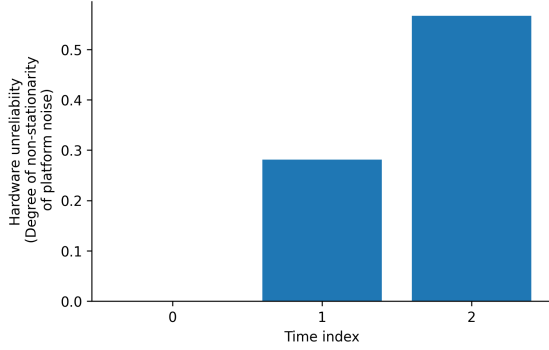


Fig. 4. We model the degradation of a non-stationary Pauli noise channel by assuming the coherence time steadily decreases over time. Using a non-stationary Dirichlet distribution, we model the joint distribution of coefficients for a two-qubit circuit, which fluctuate as coherence times deteriorate. The y-axis represents the degree of non-stationarity, and the x-axis shows four time-periods. The Hellinger distance between the Dirichlet distributions at time $\tau=0$ and a later time is a measure of non-stationarity, increasing from 0 to 57%. This model is based on transmon platforms and is used as an experimental setup for our simulation experiments.

$$E_2^{\text{APD}} = E_1^{\text{PD}} E_0^{\text{AD}} = \begin{pmatrix} 0 & 0 \\ 0 & \sqrt{[1-\gamma]\lambda} \end{pmatrix}. \quad (13)$$

Using the fact that:

$$E_0^{\text{APD}} = \frac{1 + \sqrt{1-\lambda-\gamma+\lambda\gamma}}{2} I + \frac{1 - \sqrt{1-\lambda-\gamma+\lambda\gamma}}{2} Z, \quad (14)$$

$$E_1^{\text{APD}} = \frac{\sqrt{\gamma}}{2} X + \frac{\sqrt{\gamma}}{2} iY, \quad (15)$$

$$E_2^{\text{APD}} = \frac{\sqrt{\lambda-\lambda\gamma}}{2} I - \frac{\sqrt{\lambda-\lambda\gamma}}{2} Z. \quad (16)$$

the APD channel can be expressed as:

$$\begin{aligned} \mathcal{E}^{\text{APD}}(\rho) = & \frac{2-\gamma+2\sqrt{1-\lambda-\gamma+\lambda\gamma}}{4} \rho + \frac{\gamma}{4} X\rho X - \frac{\gamma}{4} Y\rho Y \\ & + \frac{2-\gamma-2\sqrt{1-\lambda-\gamma+\lambda\gamma}}{4} Z\rho Z \\ & + \frac{\gamma}{4} I\rho Z + \frac{\gamma}{4} Z\rho I - \frac{\gamma}{4i} X\rho Y - \frac{\gamma}{4i} Y\rho X, \end{aligned} \quad (17)$$

where λ and γ are the APD parameters, and I , X , Y , and Z are the Pauli matrices.

Multi-qubit and multi-gate APD channels are not efficiently simulatable due to the Gottesman-Knill theorem [43], which states that only Pauli channels, those with Pauli matrices as their Kraus operators, can be simulated efficiently on a classical

computer. Channel twirling maps [44]–[46] a complex channel to a simpler one while preserving certain features such as the average channel fidelity and the entanglement fidelity [47]. In particular, it transforms a non-Pauli channel into the Pauli noise channel, which is widely used in quantum error correction because it is a simple and natural model for random quantum noise [48]–[50]. It is a well-understood and easily implementable noise model that can simulate a variety of realistic physical processes that lead to quantum errors, such as dephasing, amplitude damping, and phase-flip errors. Additionally, the Pauli noise channel is mathematically tractable and can be efficiently simulated, making it a useful tool for developing and testing quantum error correction protocols. It can be used to estimate the average fidelity of a quantum gate subject to the original APD channel and identify codes that work for the APD channel [49].

Thus, using the fact that the average channel fidelities of the APD and its twirled version (i.e., the Pauli noise channel) are the same, one can express the Pauli noise parameters as a function of the T_1 and T_2 times of the APD.

Pauli twirling is defined as:

$$\mathcal{E}_{\text{twirl}}(\rho) = \frac{1}{4} \sum_{A \in \{I, X, Y, Z\}} A^\dagger \mathcal{E}(A\rho A^\dagger) A. \quad (18)$$

This is a convex combination of channels and hence also a channel. Specifically, The twirled APD is a Pauli channel and hence efficiently simulatable. Its noise parameters, expressed as a function of the T_1 and T_2 times of the APD, can be used to model the noise with the APD channel while also benefiting from the simplicity of the Pauli noise channel for efficient simulations. The expression for twirled APD is:

$$\begin{aligned} \mathcal{E}_{\text{twirl}}^{\text{APD}}(\rho; T_1, T_2) = & \frac{1}{4} \sum_{A \in \{I, X, Y, Z\}} A^\dagger \mathcal{E}^{\text{APD}}(A\rho A^\dagger) A \\ = & \sum_{k=0}^3 c_k \sigma_k \rho \sigma_k, \end{aligned} \quad (19)$$

where,

$$\begin{aligned} c_1 = c_2 = & \frac{1}{4} [1 - \exp(-t/T_1)], \\ c_3 = & \frac{1}{4} [1 - \exp(-t/T_2)], \\ c_0 = & 1 - (c_1 + c_2 + c_3), \end{aligned} \quad (20)$$

and $\{\sigma_k\}_{k=0}^3 = \{I, X, Y, Z\}$ are the Pauli matrices. Note that the Pauli error probabilities c_1, c_2, c_3 are not equal to each other.

Section II discussed the random fluctuations of the decoherence times T_1 and T_2 as spatially and temporally varying stochastic processes across all time-scales. We express these fluctuations as random variables dependent on register location i and time τ :

$$T_1 = T_1(i, \tau) \quad \text{and} \quad T_2 = T_2(i, \tau). \quad (21)$$

It follows from Eq. (20) that the coefficients of the single-qubit Pauli noise channel will fluctuate randomly as temporally and spatially varying stochastic processes [14]. These random variables also depend on register location i and time τ :

$$c_0 = c_0(i, \tau), \quad c_1 = c_1(i, \tau), \quad c_2 = c_2(i, \tau), \quad c_3 = c_3(i, \tau). \quad (22)$$

B. Multi-qubit channel

TABLE I
TRUE MEANS OF THE TIME-VARYING NOISE PAULI CHANNEL COEFFICIENTS

Pauli term [qubit0 \otimes qubit1]	Period 0	Period 1	Period 2
II	0.379	0.326	0.26
IX	0.056	0.064	0.075
IY	0.056	0.064	0.075
IZ	0.076	0.078	0.079
XI	0.081	0.083	0.082
XX	0.012	0.016	0.024
XY	0.012	0.016	0.024
XZ	0.016	0.02	0.025
YI	0.081	0.083	0.082
YX	0.012	0.016	0.024
YY	0.012	0.016	0.024
YZ	0.016	0.02	0.025
ZI	0.127	0.12	0.108
ZX	0.019	0.024	0.031
ZY	0.019	0.024	0.031
ZZ	0.026	0.029	0.033

Let us characterize the effect of Pauli noise on quantum information encoded in an n -qubit register:

$$\mathcal{E}_x(\rho) = \sum_{i=0}^{N_p-1} x_i P_i(n) \rho P_i(n)^\dagger, \quad (23)$$

where $N_p = 4^n$ is the total number of Pauli coefficients and $P_i(n)$ are the n -qubit Pauli operators with coefficients subject to the conditions:

$$\sum_{i=0}^{N_p-1} x_i = 1, \quad x_i \geq 0. \quad (24)$$

To study the performance of error mitigation and correction algorithms in non-stationary NISQ devices, it is important to investigate the behavior of a non-stationary Pauli noise channel. The N_p coefficients of the Pauli operators can be considered as random variables that fluctuate spatially and temporally, denoted as $x_k = x_k(i, \tau)$, where $i = (i_1, \dots, i_n)$ identifies the register location(s) and τ is time. A prior hypothesis for the Pauli channel can be obtained by assuming channel separability,

in which case the N_p coefficients can be obtained using a direct product over n four-dimensional vectors, as shown in Eq. (25).

$$\mathbf{x} = \begin{pmatrix} c_0(i=0, \tau) \\ c_1(i=0, \tau) \\ c_2(i=0, \tau) \\ c_3(i=0, \tau) \end{pmatrix} \times \dots \times \begin{pmatrix} c_0(i=n-1, \tau) \\ c_1(i=n-1, \tau) \\ c_2(i=n-1, \tau) \\ c_3(i=n-1, \tau) \end{pmatrix}, \quad (25)$$

where \times refers to the direct product.

To incorporate correlations between qubit errors, one could still consider a separable noise model (for the simplicity of modeling the noise using single-qubit APD channels). These correlations stem from the spatial correlation function (for a fixed time τ and error type k) between qubits $i = a$ and $i = b$ on the device

$$\overline{x_k(i=a, \tau)x_k(i=b, \tau)}, \quad (26)$$

and fitting it to a pre-determined model, e.g. an exponentially decaying function (the decay constant quantifies how strongly the different qubit noises are correlated). Here, the average is taken over the realizations of the circuit. Now, since we do not really measure x_k in our circuits, instead we measure $T_1(i=a, \tau)$ and $T_2(i=a, \tau)$, we can substitute for $x_k(i=a, \tau)$ its dependence on T_1 and T_2 , given the twirling of a specific noise model (this is done analytically above for the single-qubit APD channel), and then the spatial and temporal statistical properties of T_1 and T_2 over our sample could be used to compute these qubit-qubit noise correlations. This may provide a richer characterization of the n -qubit case that goes a step beyond the standard ‘‘independent’’ noise approximation, which seems to fail for the particular IBM quantum computer (and likely all quantum computers more generally).

Note that in this analysis, there are two layers to the ‘‘independent’’ noise model that one can consider. (1) we can say that any Pauli channel satisfying Eq. (25) is an independent noise model. However, if Eq. (26) is non-zero for at least two qubits $a \neq b$, then the Pauli errors still contain classical (non-entangling) spatial correlations between them. (2) A subset of Pauli channels satisfying Eq. (25) will also nullify Eq. (26).

C. Quantifying the non-stationarity

The Pauli noise channel, although not a completely general noise model, still manages to model many practical situations. It is widely used because of two reasons: (a) it is efficiently simulatable on a classical computer (per the Gottesman-Knill theorem) and (b) when used as a proxy for physically accurate noise models (such as the amplitude and phase damping noise) which are not efficiently simulatable on a classical computer, it still manages to preserve important properties like entanglement fidelity [47].

As discussed in Section 2, the coefficients of the Pauli noise channel (henceforth referred to as the Pauli coefficients), are directly linked to the decoherence times T_1 and T_2 of the individual register elements.

These decoherence times exhibit stochastic fluctuations in time and across the register and show correlations between them. As a result, the Pauli coefficients also show strong correlations

among them. Another constraint is given by Eq. (25). Because $\sum x_i = 1$ and each $x_i \in [0, 1]$, the natural way to model the probability distribution function $f_X(x)$ of the multi-dimensional Pauli channel distribution is the Dirichlet distribution:

$$f_X(x) \equiv \text{Dirichlet}(x; \eta) := \frac{\Gamma\left(\sum_{i=0}^{N_p-1} \eta_i\right)}{\prod_{i=0}^{N_p-1} \Gamma(\eta_i)} \left(\prod_{i=0}^{N_p-1} x_i^{\eta_i-1} \right), \quad (27)$$

where $\eta \geq 0$ is the Dirichlet hyper-parameter for the Pauli channel distribution, Γ is the Gamma function, and $\int \text{Dirichlet}(x; \eta) dx = 1$.

^x As discussed in the previous two sections, the distribution of the decoherence times fluctuates with time. Thus, the distribution of the Pauli coefficients (i.e. the Dirichlet distribution), changes with time. Specifically, the coefficients η_i will vary with time. The distribution may be represented as $f_X(x; \tau)$. At any time instant (or at any circuit execution instance), the Pauli coefficient vector x represents a specific realization of the random variable X , which is sampled from $f_X(x; \tau)$.

Recall that we measure reliability using the Hellinger distance H_d between the distribution of the parameters characterizing the noise (in this case, the Pauli coefficients). The Hellinger distance between two time-varying Dirichlet distributions (parameterized by η and η'), quantifies the degree of non-stationarity:

$$\begin{aligned} H_d &:= \sqrt{1 - BC}, \\ BC &:= \int_x \sqrt{f(x)g(x)} dx \\ &= \frac{\Gamma\left(\sum_{i=0}^{N_p-1} \eta_i\right) \Gamma\left(\sum_{i=0}^{N_p-1} \eta'_i\right)}{\prod_{i=0}^{N_p-1} \sqrt{\Gamma(\eta_i)\Gamma(\eta'_i)}} \times \frac{\prod_{i=0}^{N_p-1} \Gamma\left(\frac{\eta_i + \eta'_i}{2}\right)}{\Gamma\left(\frac{\sum_{i=0}^{N_p-1} \eta_i + \eta'_i}{2}\right)}, \end{aligned} \quad (28)$$

where $N_p = 4^n$ and BC is the Bhattacharya coefficient.

IV. BAYESIAN INFERENCE OF STOCHASTIC PAULI NOISE

Bayesian statistical models treat unknowns as random variables and require a prior, while frequentist statistical models treat unknowns as parameters and rely solely on a data generating model. Bayesian estimators rely on the posterior for inference. Adaptive estimation using Bayesian inference can improve the performance of error mitigation schemes in the presence of time-varying noise. This approach updates the system noise hypothesis as new information becomes available. Bayesian updating is particularly important for Probabilistic Error Cancellation (discussed in the next section) when dealing with time-varying noise.

In particular, the time-varying Dirichlet distribution of the Pauli coefficient should be dynamically estimated to be able to mitigate errors more accurately. Dynamic estimation can

be done either through a point-in-time update, which uses maximum likelihood estimation, or a Bayesian inference-based rolling update. The Bayesian method is especially useful when dealing with sparse data. Bayesian inference of the Pauli noise channel is simply an application of Bayes' rule:

$$f_X(x|\text{observed data}) \propto f_X(\text{observed data}|x) f_X^{\text{prior}}(x). \quad (29)$$

The prior distribution for the Pauli channel coefficients is given by:

$$\begin{aligned} x &\sim f_X^{\text{prior}}(x) = \text{Dirichlet}(x; \eta) \\ &= \frac{\Gamma\left(\sum_{j=0}^{N_p-1} \eta_j\right)}{\prod_{j=0}^{N_p-1} \Gamma(\eta_j)} \left(\prod_{j=0}^{N_p-1} x_j^{\eta_j-1} \right). \end{aligned} \quad (30)$$

We generate our data set by executing the quantum circuit L times and recording the outcome s of the circuit measurement POVM $\{\Pi_s\}$, where s is an integer representing the observed n -bit long binary string. The data set is represented by the set $\{s_l\}$ where $l \in 0, \dots, L-1$. Each execution of the circuit results in a specific outcome s . The random variable S follows a discrete distribution from the range of $0, \dots, N-1$ with probabilities p_0, p_1, \dots, p_{N-1} , where $N = 2^n$ is the Hilbert space dimension. Also:

$$p_s = \text{Tr}[\Pi_s \tilde{\mathcal{G}}_x(\rho_{\text{test}})], \quad (31)$$

where $\tilde{\mathcal{G}}_x$ is a noisy implementation of the ideal quantum operation \mathcal{G} characterized by the noise parameter x and ρ_{test} is a known test density matrix.

Assuming circuit runs are independent of each other, the likelihood function is given by:

$$\text{Pr}(\{s_l\}|x) = \prod_{i=0}^{N-1} \left[\text{Tr}[\Pi_i \tilde{\mathcal{G}}_x(\rho_{\text{test}})] \right]^{C_i(\{s_l\})}, \quad (32)$$

where, $C_i(\{s_l\}) = \sum_{\ell=0}^{L-1} \delta_i(s_\ell)$ (with $i \in \{0, 1, \dots, N-1\}$) is simply a counter function that counts how many times i appeared in the experimentally observed data post-measurement ($\delta_i(s)$ is Kronecker delta function which is 1 if $i = s$ and zero otherwise). The log of the posterior is then given by:

$$\begin{aligned} \log f_X^{\text{posterior}}(x|\text{data}) &= \sum_{i=0}^{N-1} C_i(\text{data}) \log \left[\text{Tr}[\Pi_i \tilde{\mathcal{G}}_x(\rho_{\text{test}})] \right] \\ &\quad + \sum_{j=0}^{N_p-1} (\eta_j - 1) \log x_j \\ &\quad + \text{terms independent of } x. \end{aligned} \quad (33)$$

Lastly, the Maximum-a-posterior (MAP) estimate is obtained as:

$$\hat{x}(\tau) = \underset{x}{\operatorname{argmax}} \left[\sum_{i=0}^{N-1} C_i(\text{data}) \log \left[\operatorname{Tr}[\Pi_i \tilde{\mathcal{G}}_x(\rho_{\text{test}})] \right] + \sum_{j=0}^{N_p-1} (\eta_j - 1) \log x_j \right]. \quad (34)$$

A. Example application: PEC on unreliable platforms

1) *Method*: Probabilistic error cancellation (PEC) is a well-known error mitigation method [34], [35], [51]. The four broad steps of the PEC workflow are as follows. We use the convention that calligraphic symbols denote super-operators acting on density matrices:

$$\mathcal{G}(\rho) = \bar{G}\rho G^\dagger. \quad (35)$$

First, expand an ideal unitary gate \mathcal{G} as a (noise-model dependent) linear combination of implementable noisy gate set $\{\tilde{\mathcal{G}}_j\}$ (with its ideal counterpart $\{\mathcal{G}_j\}$), as follows:

$$\mathcal{G} = \sum_{j=0}^{N_p-1} \theta_j \tilde{\mathcal{G}}_j, \quad (36)$$

where θ_j are real coefficients, and \mathcal{E}_x is an error channel (such as Pauli noise channel), and $\tilde{\mathcal{G}}_j \equiv \mathcal{E}_x \circ \mathcal{G}_j$. For example, if $G = H \otimes H$ is a two-qubit Hadamard gate, then the noisy basis circuits are given by

$$\tilde{\mathcal{G}}_{\sigma\sigma'} = \mathcal{E}_x \circ \mathcal{P}_{\sigma\sigma'} \circ \mathcal{G} \quad (37)$$

where $\mathcal{P}_{\sigma\sigma'}(\cdot) \equiv (\sigma \otimes \sigma')(\cdot)(\sigma \otimes \sigma')$, and σ, σ' are picked from the set of Pauli matrices $\{I, X, Y, Z\}$.

The second step of PEC involves using a measurement-based estimation procedure to estimate the expectation value of the mitigated operator as $\sum_{j=0}^{N_p-1} \theta_j \langle \tilde{\mathcal{G}}_j \rangle$. To improve computational efficiency, we sample an implementable gate from the quasi-probability representation of the ideal gate, using a probabilistic approximation with Monte Carlo importance sampling. The ideal gate can be approximated as:

$$\mathcal{G} = \sum_{w=0}^{N_p-1} p(w) [\Theta \operatorname{sgn}(\theta_w) \tilde{\mathcal{G}}_w], \quad (38)$$

where

$$\Theta = \sum_{w=0}^{N_p-1} |\theta_w| \quad (39)$$

and $p(w) = |\theta_w|/\Theta$ and w is a random variable such that $w \in 0, 1, \dots, N_p - 1$. The procedure gives more weight to coefficients θ_w with larger magnitudes. The key fact behind PEC is that, given the random variable \tilde{w} , the probabilistic super-operator $\Theta \operatorname{sgn}(\theta_w) \tilde{\mathcal{G}}_w$ is an unbiased estimator for the ideal gate \mathcal{G} , i.e. $\mathcal{G} = \mathbb{E}_w [\Theta \operatorname{sgn}(\theta_w) \tilde{\mathcal{G}}_w]$.

The third step of PEC involves sampling an implementable circuit from the quasi-probability representation of an ideal

circuit. This is achieved by sampling from the quasi-probability representation of each ideal gate of the circuit, multiplying the sign of each sampled gate to obtain the global sign associated with the full circuit, and multiplying the Θ of each sampled gate to obtain the global Θ associated with the full circuit. This produces an unbiased estimator of the ideal circuit, and the sampling average of the circuit estimator converges (in the limit of many samples) to the ideal circuit, similar to the previous case of a single-gate estimator.

The final step of PEC involves inferring an ideal expectation value from the noisy execution of the sampled circuits. In our 2-qubit example application, we take the observables as the projector on the computation basis states to infer the ideal histogram. There are four projectors, namely $\Pi_0 = |00\rangle\langle 00|$, $\Pi_1 = |01\rangle\langle 01|$, $\Pi_2 = |10\rangle\langle 10|$, and $\Pi_3 = |11\rangle\langle 11|$, each representing a computation basis state. To obtain a mitigated estimate of the ideal probability associated with a basis state, one needs to sample many circuits from the quasi-probability representation of the ideal circuit, execute all the samples with the noisy executor, and obtain a list of noisy expectation values for each projector. Then, by averaging with suitable weights (signs and Θ), the ideal histogram can be obtained.

We immediately note that PEC provides the ideal circuit in the asymptotic Monte Carlo circuit limit if the noise is static and perfectly characterized, which does not require updating the PEC implementation. However, in the presence of non-stationary time-varying noise distributions, an adaptive approach becomes necessary.

2) *Simulation setup*: The time-variation in the Pauli noise channel on the transmon platform highlights its unreliability. This poses challenges for any algorithm that relies on accurate noise characterization, including probabilistic error cancellation (PEC), which suffers from such reliability issues.

PEC is a method for approximating the noiseless ideal sub-system of an unknown circuit made up of smaller modular sub-systems such as CNOT, X, Y, Z, and Hadamard gates. By generating and averaging many Monte Carlo circuits, we can construct a "noiseless ideal sub-system" which can be used to implement a bigger circuit. PEC assumes an effective noise model that affects basis circuits. These noisy basis circuits are assumed to be implemented perfectly, as detailed in [34], [52]. Therefore, accurately characterizing the noise is crucial for successful PEC implementation. The time-varying noise in the platform makes the basis circuit set used by PEC itself time-varying, requiring adaptive channel estimation each time.

In this section, our goal is to implement a noiseless, ideal operation on two qubits in the presence of time-varying noise using adaptive estimation and probabilistic error cancellation. Specifically, we aim to execute a Hadamard operation on qubit 0 and qubit 1, denoted as $H \otimes H$, when only noisy basis gates are available. This is achieved in the presence of general, non-separable, time-varying Pauli noise channel.

3) *Time-varying Pauli noise*: In our simulation, we consider a two-qubit register subject to time-varying noise. The experimental data and causes of the decoherence fluctuations are discussed in Section II. The data used in our experiment

was obtained from a transmon device called Belem by IBM in December 19, 2022.

We assume that the mean of the stochastic T_1 coherence time for the first qubit decreases uniformly in a simple step-function-like manner over five time periods, deteriorating from 150 to 60 μs . Similarly, for the second qubit, we assume that the mean of the stochastic T_1 coherence time deteriorates from 200 to 10 μs in five time periods. Additionally, we assume a simple step-function-like decrease in the mean of the stochastic T_2 coherence time for the first qubit, deteriorating from 70 to 50 μs in five time periods. Finally, for the second qubit, we assume that the mean of the stochastic T_2 coherence time will deteriorate from 130 to 62.5 μs in five time periods. The coefficients of the Pauli channel are then computed using Eq. (20). This setup models the performance when the non-identity Pauli channel coefficients increases with time, such as in between calibrations. We assume a typical execution time of 100 μs for the Hadamard gate on the IBM transmon platform.

We investigate the non-stationarity of the time-varying Pauli noise channel in our simulation where the register coherence time decreases steadily with time. We model the joint distribution of the coefficients using a non-stationary Dirichlet distribution, which varies with time. The Hellinger distance between the Dirichlet distribution at time $\tau=0$ and a later time is a measure of the degree of non-stationarity, increasing from 0 to 57% as shown in Fig. 4. The true means of the time-varying noise Pauli channel coefficients are shown in Table I.

In period 0, the coefficient of the identity term in the Pauli noise channel is 38%, but by period 2, it degrades to 26%. This change is driven by the deterioration in the coherence times for qubit 0 and qubit 1, respectively, as described above. We use the Hellinger distance to maintain consistency with the Bayesian inference section as the Dirichlet distribution will be used later in this study.

4) *Initial time period:* At the outset, we assume we are in period 0, equipped with accurate knowledge of the Pauli noise channel. With this knowledge, we obtain the super-operator expression for the noisy basis circuits, which we linearly combine to estimate the ideal operation ($H \otimes H$). This linear combination is almost error-free, as long as the noisy basis circuits expressed as super-operators are completely positive and trace preserving (CPTP). Post importance sampling using the PEC procedure, we obtain almost error-free results for the mean of the observable. The reconstructed operation is a weighted average using a quasi-probability distribution that uses the true noisy basis. Our results, shown in Fig. 5 (b), indicate an accurate ideal gate implementation in the presence of noise in period 0, with a Hellinger distance between the expected and observed output of 0.34%. This small error stems from the finite Markov chain Monte Carlo (MCMC) circuit samples.

5) *Subsequent time periods:* In subsequent time periods, the noise characteristics of the Pauli channel change as shown in Fig. 4 and Table I. This change renders the previously implemented PEC approach inaccurate as the super-operators

characterizing the noisy basis circuits are no longer accurate. Without adaptive mitigation, two issues arise: the old linear combination coefficients for importance sampling of the Monte-Carlo circuits are no longer valid, and the circuits, post generation, are impacted by new types of noise during execution. The black bars in Fig. 5 (b) indicate that the Hellinger distance between the output and ideal increases from 0.34% to 7%, and 15% in periods 1, and 2, respectively. To examine the raw data of the obtained histograms for the non-adaptive case, refer to the crimson colored bars in Fig. 5 (a).

TABLE II
ESTIMATED PAULI COEFFICIENTS FOR PEIOD 1

Pauli term [qubit0 \otimes qubit1]	Estimated value	True value
II	0.311	0.326
IX	0.064	0.064
IY	0.064	0.064
IZ	0.097	0.078
XI	0.078	0.083
XX	0.016	0.016
XY	0.016	0.016
XZ	0.024	0.02
YI	0.078	0.083
YX	0.016	0.016
YY	0.016	0.016
YZ	0.024	0.02
ZI	0.114	0.12
ZX	0.023	0.024
ZY	0.023	0.024
ZZ	0.036	0.029

TABLE III
ESTIMATED COEFFICIENTS FOR PERIOD 2

Pauli term [qubit0 \otimes qubit1]	Estimated value	True value
II	0.243	0.26
IX	0.073	0.075
IY	0.073	0.075
IZ	0.103	0.079
XI	0.074	0.082
XX	0.022	0.024
XY	0.022	0.024
XZ	0.031	0.025
YI	0.074	0.082
YX	0.022	0.024
YY	0.022	0.024
YZ	0.031	0.025
ZI	0.103	0.108
ZX	0.031	0.031
ZY	0.031	0.031
ZZ	0.044	0.033

6) *Adaptive estimation:* To improve the accuracy of the PEC-based circuit implementation in the presence of time-varying noise characteristics, we utilize Bayesian inference for dynamic channel estimation. Bayesian inference can require fewer samples than maximum likelihood to produce reliable parameter estimates, provided that the prior specification is of high quality and the model complexity is not too high.

For the Bayesian update, we use the histogram of projective measurements obtained from applying the old PEC circuit to a test density matrix, as shown in Eq. (40). This test density

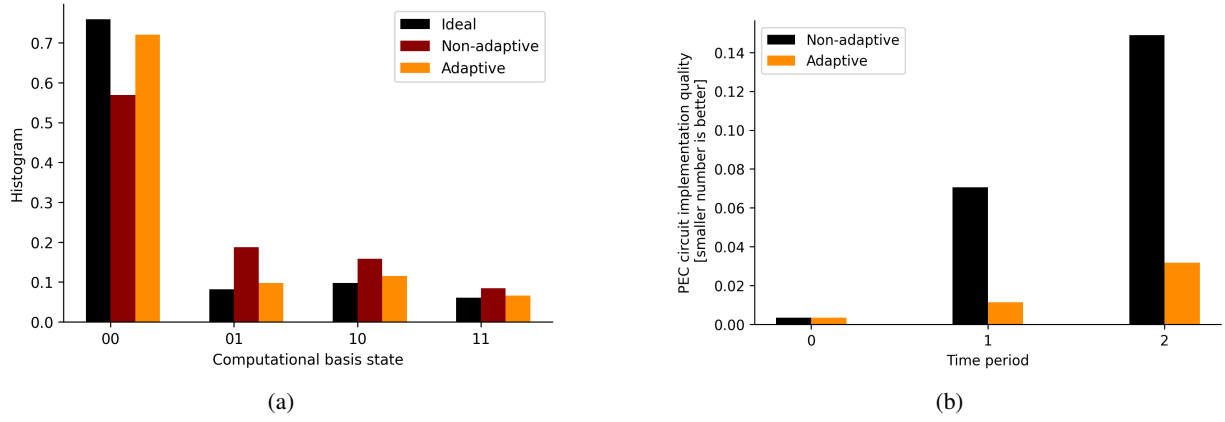


Fig. 5. (a) This graph compares adaptive and non-adaptive PEC for the $H \otimes H$ gate under time-varying noise. The y-axis shows the probability of observing a basis state. The black bars represent the ideal histogram for the test input from Eq. (40), while red/orange bars are non-adaptive PEC results. Adaptive PEC improves accuracy. For example, the $|00\rangle$ probability increases from 57% to 72%. (b) This graph compares adaptive and non-adaptive PEC implementations over four time-periods with time-varying noise, using Hellinger distance to measure the difference from the ideal distribution. The black and orange bars represent the observed distributions with non-adaptive and adaptive PEC, respectively. Adaptive PEC significantly outperforms non-adaptive PEC in reducing Hellinger distance to 1.1%, and 3.2% compared to 7%, and 15% for non-adaptive PEC across time-periods. Adaptive PEC uses adaptive estimation of noise super-operators to improve accuracy compared to non-adaptive PEC. Time-varying noise underscores the need for adaptive PEC.

matrix represents a known 2-qubit quantum state that produces an uneven probability distribution, which is important for accurately estimating the Pauli coefficients later. The resulting stream of 2-bit strings belongs to one of four possibilities: 00, 01, 10, 11 with corresponding probabilities as 0.76, 0.08, 0.10, and 0.06, respectively. The test density matrix can be replaced with any reliably prepared quantum state that has sufficient off-diagonal components to produce a rich histogram.

$$\rho_{\text{test}} = \begin{pmatrix} 0.2 & 0.22 - 0.02j & 0.15 - 0.09j & 0.16 - 0.1j \\ 0.22 + 0.02j & 0.24 & 0.16 - 0.08j & 0.19 - 0.1j \\ 0.15 + 0.09j & 0.16 + 0.08j & 0.36 & 0.14 + 0.06j \\ 0.16 + 0.1j & 0.19 + 0.1j & 0.14 - 0.06j & 0.21 \end{pmatrix}. \quad (40)$$

Fig. 5 (b) compares the performance of adaptive and non-adaptive PEC implementations across four back-to-back time-periods in the presence of time-varying noise. The y-axis represents the Hellinger distance, which is the distance between two discrete probability distributions over the computational basis states. The black bars show the experimentally observed distribution when non-adaptive PEC is used, while the orange bars show the distribution when adaptive PEC is used. The x-axis represents the four time-periods. When using non-adaptive PEC, the Hellinger distance from the ideal distribution is 7%, and 15% for time-periods 1, and 2, respectively. When using adaptive PEC, the Hellinger distance significantly improves to 1.1%, and 3.1% for the same time-periods. This graph demonstrates that adaptive PEC improves the accuracy of the PEC circuit implementation in the presence of time-varying noise compared to non-adaptive PEC. The improvement can be attributed to the fact that the noise characteristics of the Pauli channel change over time, becoming increasingly worse. As a result, the previously implemented PEC circuits become inaccurate since the super-operators characterizing the noisy

basis circuits are no longer valid. Without adaptive mitigation, two issues arise: the old linear combination coefficients for importance sampling of the Monte-Carlo circuits become invalid, and new types of noise during execution affect the circuits post-generation. This underscores the need for adaptive PEC, which uses adaptive estimation of the noise super-operators to address these issues and improve accuracy in the presence of time-varying noise.

The posterior distribution, a 16-dimensional Dirichlet distribution over the Pauli noise channel coefficients, is used to estimate the MAP (maximum-a-posteriori) of the coefficients. Table II and Table III demonstrate the MAP estimation performance at granularity of individual Pauli coefficients and illustrates the quality of Bayesian estimation. With this new knowledge, we estimate the super-operators for the noisy basis circuits and the linear combination of these super-operators to design the actual circuits. The PEC is then implemented using the estimated super-operators, resulting in improved output quality, as shown in Fig. 5 (a) which compares the output distribution over computational basis states for adaptive and non-adaptive PEC in the presence of time-varying noise. In this figure, the y-axis represents the probability of observing a particular computational basis state. In this two-qubit case, there are four possible states, and their probabilities sum to 1. The black bars indicate the ideal probabilities, while the red and orange bars represent the probabilities obtained with non-adaptive and adaptive PEC, respectively, for the fourth time-period. The graph demonstrates that adaptive PEC, which used adaptive estimation of the noise super-operators, improves accuracy compared to non-adaptive PEC. Specifically, the probability of observing 00 in period 2 increases from 57% for non-adaptive PEC to 72% for adaptive PEC in the presence of time-varying noise.

Note that we used a Pauli noise channel with all 4^n terms.

However, in practical applications, it becomes necessary to reduce the number of terms. To achieve this, one can explore the use of a sparse Lindbladian noise model [53], which considers noise only in nearest-neighbor connections for Pauli terms with weight greater than 1. This reduction in terms leads to a linear scaling instead of exponential with the number of qubits, making the model more computationally efficient. Also note that while it has been observed that single-qubit gate noise can be more than 10 times smaller than two-qubit gate noise [53], it cannot be disregarded in Probabilistic Error Cancellation (PEC) due to error propagation effects. Moreover, in the presence of time-varying quantum noise, it becomes even more critical to account for single-qubit noise to ensure accurate error cancellation.

Note that recalibrating the noise model does not solve the challenge of dynamic estimation, as experimental evidence from various studies indicates significant fluctuations in decoherence times over time. These fluctuations, observed in studies like [38], [39], show that decoherence times can vary by approximately 50% within an hour due to the presence of oxides on superconductors' surfaces, represented as fluctuating two-level systems (TLS) [1], [2]. These fluctuations at the scale of minutes and hours are considered non-systematic noise, which cannot be addressed solely through re-calibrations. This emphasizes the necessity for time-varying adaptive algorithms. In contrast to methods focused on re-calibration, our approach is more versatile, applicable to situations where incomplete knowledge of the noise parameters (e.g. Pauli weights) is unavoidable, regardless of the source of imperfection or inaccuracy, be it systematic or non-systematic noise.

V. CONCLUSION

In this study, we explore the spatio-temporal stochasticity of the Pauli noise channel, which captures the non-stationarity of the quantum noise in superconducting qubits. We present the variation of the coefficients of the noise channel for IBM Belem. We use a Dirichlet distribution to model the joint distribution of the coefficients of the Pauli noise channel. The Hellinger distance between two time-varying Dirichlet distributions quantifies the degree of non-stationarity, which is used to measure reliability of error channel characterization. We characterize the effect of the time-varying Pauli noise on the quantum information encoded in an n -qubit register and show how to obtain the coefficients of a separable 2-qubit Pauli noise channel. These coefficients are directly linked to the decoherence times of individual register elements, which exhibit stochastic fluctuations in time and across the register, leading to strong correlations among the Pauli coefficients.

The probabilistic error cancellation (PEC) technique of quantum error mitigation provides an ideal circuit in the asymptotic Monte Carlo circuit limit if the noise is perfectly characterized. However, in the presence of non-stationary time-varying noise, an adaptive approach becomes necessary. We propose an adaptive Bayesian inference approach to improve the performance of PEC for an unreliable platform affected by time-varying noise. The time-varying Dirichlet distribution of

the Pauli coefficients is dynamically estimated using a Bayesian inference-based rolling update. We present an application of PEC for executing a Hadamard operation on two-qubits in the presence of time-varying noise using adaptive estimation. The results of the simulation indicate that the previously implemented PEC approach becomes inaccurate with the change in the noise characteristics of the Pauli channel. Without adaptive mitigation, two issues arise: the old linear combination coefficients for importance sampling of the Monte-Carlo circuits are no longer valid, and the circuits, post-generation, are impacted by new types of noise during execution. The output implementation is severely affected. Overall, this study provides important insights into the behavior of non-stationary noise channels based on real-world quantum computing platforms.

In this study, we considered the spatial correlations for multi-qubit noise by treating the latter as a separable collection of single-qubit channels, while retaining the spatial correlations between the different single-qubit T_1 and T_2 times. A more general approach would be to consider non-separable multi-qubit noise channels, with collective T_1 and T_2 times. This will allow us to capture non-classical correlations between qubits due to the entangling nature of multi-qubit noise and understand their effects on the performance of the PEC method. The focus of this work was on the adaptive implementation of PEC. However, the quantum estimation procedure that is implicitly involved in this discussion could be addressed in more detail. This work utilized adaptive algorithms with Bayesian inference and a Dirichlet prior to achieve probabilistic error cancellation in the presence of time-varying quantum noise. Real-world noise data from quantum devices was used for simulations. Future research may explore the implications of metrological bounds [19] on multi-parameter quantum estimation using quantum Fisher information techniques for practical applications. Additionally, future investigations aim to validate and demonstrate the algorithm's efficacy with an actual quantum device.

The conventional PEC method faces challenges in scalability due to its preference for a complete noise characterization to achieve maximum accuracy [34]. To address this, some suggestions have been made to enhance tractability by reducing the number of parameters that require estimation. One approach involves reducing overhead in quasi-probability representation construction by omitting terms dependent on the noise coefficient magnitude. This approach allows for better scalability but comes at the expense of accuracy, leaving the user to decide their tolerance for inaccuracy. Another suggested approach, as presented in [53], increases reproducibility by removing the user's freedom to set the inaccuracy tolerance. It involves using sparse Lindbladian models, assuming only qubits with physical connections experience noise, leading to linear resource estimation costs instead of exponential. The adaptive approach we propose is model-agnostic and can be used with sparse Lindbladian models. The scalability, therefore, depends on the nature of the effective model deployed, with our approach being blind to these specifics.

Noise characterizations are assumed to be constant in current

research in quantum computing when applying error mitigation. Thus, a natural question arises as to how sensitive the output is to variable noise processes. In this study, we have used an adaptive scheme using Bayesian inference to dynamically estimate the noise channels, and used that knowledge to compensate the error. This helps stabilize the circuit in terms of minimizing fluctuations with respect to the time-varying noise. The algorithm does not require a-priori knowledge of channel calibration. In fact, erroneous channel calibration knowledge is acceptable too - as the method learns dynamically from the measurements (binary strings) observed. Our work fills a gap for utilizing unstable quantum platforms with the goal of improving reproducibility in the burgeoning field of quantum information science.

ACKNOWLEDGMENTS

We thank the anonymous reviewers for their helpful feedback. This work is supported by the U. S. Department of Energy (DOE), Office of Science, National Quantum Information Science Research Centers, Quantum Science Center and the Advanced Scientific Computing Research, Advanced Research for Quantum Computing program, and the U.S. Army Research Office through the U.S. MURI Grant No. W911NF-18-1-0218. This research used computing resources of the Oak Ridge Leadership Computing Facility, which is a DOE Office of Science User Facility supported under Contract DE-AC05-00OR22725. The manuscript is authored by UT-Battelle, LLC under Contract No. DE-AC05-00OR22725 with the U.S. Department of Energy. The U.S. Government retains for itself, and others acting on its behalf, a paid-up nonexclusive, irrevocable worldwide license in said article to reproduce, prepare derivative works, distribute copies to the public, and perform publicly and display publicly, by or on behalf of the Government. The Department of Energy will provide public access to these results of federally sponsored research in accordance with the DOE Public Access Plan: <http://energy.gov/downloads/doe-public-access-plan>.

REFERENCES

- [1] Clemens Müller, Jürgen Lisenfeld, Alexander Shnirman, and Stefano Poletto. Interacting two-level defects as sources of fluctuating high-frequency noise in superconducting circuits. *Physical Review B*, 92(3):035442, 2015.
- [2] PV Klimov, Julian Kelly, Z Chen, Matthew Neeley, Anthony Megrant, Brian Burkett, Rami Barends, Kunal Arya, Ben Chiaro, Yu Chen, et al. Fluctuations of energy-relaxation times in superconducting qubits. *Physical review letters*, 121(9):090502, 2018.
- [3] Sergey Bravyi, Sarah Sheldon, Abhinav Kandala, David C McKay, and Jay M Gambetta. Mitigating measurement errors in multiqubit experiments. *Physical Review A*, 103(4):042605, 2021.
- [4] Martin Kliesch and Ingo Roth. Theory of quantum system certification. *PRX Quantum*, 2(1):010201, 2021.
- [5] Peter V Coveney, Derek Groen, and Alfons G Hoekstra. Reliability and reproducibility in computational science: implementing validation, verification and uncertainty quantification in silico. *Philosophical Transactions of the Royal Society A*, 379(2197):20200409, 2021.
- [6] Monya Baker. 1,500 scientists lift the lid on reproducibility. *Nature*, 533(7604), 2016.
- [7] James D Nichols, Madan K Oli, William L Kendall, and G Scott Boomer. Opinion: A better approach for dealing with reproducibility and replicability in science. *Proceedings of the National Academy of Sciences*, 118(7), 2021.
- [8] Robin Blume-Kohout. Optimal, reliable estimation of quantum states. *New Journal of Physics*, 12(4):043034, 2010.
- [9] Samuele Ferracin, Seth T Merkel, David McKay, and Animesh Datta. Experimental accreditation of outputs of noisy quantum computers. *arXiv preprint arXiv:2103.06603*, 2021.
- [10] John Preskill. Quantum computing in the nisq era and beyond. *Bulletin of the American Physical Society*, 64, 2019.
- [11] Timothy Proctor, Melissa Revelle, Erik Nielsen, Kenneth Rudinger, Daniel Lobser, Peter Maunz, Robin Blume-Kohout, and Kevin Young. Detecting and tracking drift in quantum information processors. *Nature communications*, 11(1):1–9, 2020.
- [12] Marko Znidaric. Stability of quantum dynamics. *arXiv preprint quant-ph/0406124*, 2004.
- [13] Haimeng Zhang, Bibek Pokharel, EM Levenson-Falk, and Daniel Lidar. Predicting non-markovian superconducting qubit dynamics from tomographic reconstruction. *arXiv preprint arXiv:2111.07051*, 2021.
- [14] Josu Etxezarreta Martinez, Patricio Fuentes, Pedro Crespo, and Javier Garcia-Frias. Time-varying quantum channel models for superconducting qubits. *npj Quantum Information*, 7(1):1–10, 2021.
- [15] Cristian Bonato and Dominic W Berry. Adaptive tracking of a time-varying field with a quantum sensor. *Physical Review A*, 95(5):052348, 2017.
- [16] Luis Cortez, Areeya Chantasri, Luis Pedro García-Pintos, Justin Dressel, and Andrew N Jordan. Rapid estimation of drifting parameters in continuously measured quantum systems. *Physical Review A*, 95(1):012314, 2017.
- [17] Timothy Proctor, Melissa Revelle, Erik Nielsen, Kenneth Rudinger, Daniel Lobser, Peter Maunz, Robin Blume-Kohout, and Kevin Young. Detecting, tracking, and eliminating drift in quantum information processors. *arXiv preprint arXiv:1907.13608*, 2019.
- [18] Shu-Hao Wu, Ethan Turner, and Hailin Wang. Continuous real-time sensing with a nitrogen-vacancy center via coherent population trapping. *Physical Review A*, 103(4):042607, 2021.
- [19] Arshag Danageozian, Ashe Miller, Pratik J Barge, Narayan Bhusal, and Jonathan P Dowling. Noisy coherent population trapping: applications to noise estimation and qubit state preparation. *Journal of Physics B: Atomic, Molecular and Optical Physics*, 55(15):155503, 2022.
- [20] Ethan Turner, Shu-Hao Wu, Xinzhu Li, and Hailin Wang. Spin-based continuous bayesian magnetic-field estimations aided by feedback control. *Physical Review A*, 106(5):052603, 2022.
- [21] Swarnadeep Majumder, Leonardo Andreta de Castro, and Kenneth R Brown. Real-time calibration with spectator qubits. *npj Quantum Information*, 6(1):19, 2020.
- [22] Arshag Danageozian. Recovery with incomplete knowledge: Fundamental bounds on real-time quantum memories. *arXiv preprint arXiv:2208.04427*, 2022.
- [23] Hongting Song, Areeya Chantasri, Behnam Tonekaboni, and Howard M Wiseman. Optimized mitigation of random-telegraph-noise dephasing by spectator-qubit sensing and control. *Physical Review A*, 107(3):L030601, 2023.
- [24] Hyukjoon Kwon, Rick Mukherjee, and MS Kim. Reversing lindblad dynamics via continuous petz recovery map. *Physical Review Letters*, 128(2):020403, 2022.
- [25] José Lebreuilly, Kyungjoo Noh, Chiao-Hsuan Wang, Steven M Girvin, and Liang Jiang. Autonomous quantum error correction and quantum computation. *arXiv preprint arXiv:2103.05007*, 2021.
- [26] Rochus Klesse and Sandra Frank. Quantum error correction in spatially correlated quantum noise. *Physical review letters*, 95(23):230503, 2005.
- [27] Riddhi Swaroop Gupta, Luke CG Govia, and Michael J Biercuk. Integration of spectator qubits into quantum computer architectures for hardware tune-up and calibration. *Physical Review A*, 102(4):042611, 2020.
- [28] Pedro Parrado-Rodríguez, Ciarán Ryan-Anderson, Alejandro Bermudez, and Markus Müller. Crosstalk suppression for fault-tolerant quantum error correction with trapped ions. *Quantum*, 5:487, 2021.
- [29] Chao Fang, Ye Wang, Shilin Huang, Kenneth R Brown, and Jungsang Kim. Crosstalk suppression in individually addressed two-qubit gates in a trapped-ion quantum computer. *Physical Review Letters*, 129(24):240504, 2022.
- [30] Joseph M Lukens, Kody JH Law, Ajay Jasra, and Pavel Lougovski. A practical and efficient approach for bayesian quantum state estimation. *New Journal of Physics*, 22(6):063038, 2020.
- [31] Muqing Zheng, Ang Li, Tamás Terlaky, and Xiu Yang. A bayesian approach for characterizing and mitigating gate and measurement errors. *arXiv preprint arXiv:2010.09188*, 2020.
- [32] Neil J Gordon, David J Salmond, and Adrian FM Smith. Novel approach to nonlinear/non-gaussian bayesian state estimation. In *IEE Proceedings F-radar and signal processing*, volume 140, pages 107–113. IET, 1993.
- [33] Jayesh H Kotecha and Petar M Djuric. Gaussian sum particle filtering. *IEEE Transactions on signal processing*, 51(10):2602–2612, 2003.

- [34] Kristan Temme, Sergey Bravyi, and Jay M Gambetta. Error mitigation for short-depth quantum circuits. *Physical Review Letters*, 119(18):180509, 2017.
- [35] Suguru Endo, Simon C Benjamin, and Ying Li. Practical quantum error mitigation for near-future applications. *Physical Review X*, 8(3):031027, 2018.
- [36] Richard Hughes and Todd Heinrichs. A quantum information science and technology roadmap. *Rep. LA-UR-04-1778, ARDA*, 2004.
- [37] Dephasing and relaxation. available online: <https://wright.chem.wisc.edu/content/dephasing-and-relaxation-0/> (accessed on 2 dec 2022).
- [38] Malcolm Carroll, Sami Rosenblatt, Petar Jurcevic, Isaac Lauer, and Abhinav Kandala. Dynamics of superconducting qubit relaxation times. *arXiv preprint arXiv:2105.15201*, 2021.
- [39] Corey Rae H McRae, Gregory M Stiehl, Haozhi Wang, Sheng-Xiang Lin, Shane A Caldwell, David P Pappas, Josh Mutus, and Joshua Combes. Reproducible coherence characterization of superconducting quantum devices. *Applied Physics Letters*, 119(10):100501, 2021.
- [40] JH Béjanin, CT Earnest, AS Sharafeldin, and M Mariantoni. Interacting defects generate stochastic fluctuations in superconducting qubits. *Physical Review B*, 104(9):094106, 2021.
- [41] Jonathan J Burnett, Andreas Bengtsson, Marco Scigliuzzo, David Niepce, Marina Kudra, Per Delsing, and Jonas Bylander. Decoherence benchmarking of superconducting qubits. *npj Quantum Information*, 5(1):1–8, 2019.
- [42] Michael A Nielsen and Isaac Chuang. Quantum computation and quantum information, 2002.
- [43] Daniel Gottesman. The heisenberg representation of quantum computers. *arXiv preprint quant-ph/9807006*, 1998.
- [44] Tilo Eggeling and Reinhard F Werner. Separability properties of tripartite states with $u \otimes u \otimes u$ symmetry. *Physical Review A*, 63(4):042111, 2001.
- [45] Christoph Dankert, Richard Cleve, Joseph Emerson, and Etera Livine. Exact and approximate unitary 2-designs and their application to fidelity estimation. *Physical Review A*, 80(1):012304, 2009.
- [46] Easwar Magesan. Gaining information about a quantum channel via twirling. Master’s thesis, University of Waterloo, 2008.
- [47] Michał Horodecki, Paweł Horodecki, and Ryszard Horodecki. General teleportation channel, singlet fraction, and quasidistillation. *Physical Review A*, 60(3):1888, 1999.
- [48] Joseph Emerson, Marcus Silva, Osama Moussa, Colm Ryan, Martin Laforest, Jonathan Baugh, David G Cory, and Raymond Laflamme. Symmetrized characterization of noisy quantum processes. *Science*, 317(5846):1893–1896, 2007.
- [49] Marcus Silva, Easwar Magesan, David W Kribs, and Joseph Emerson. Scalable protocol for identification of correctable codes. *Physical Review A*, 78(1):012347, 2008.
- [50] Josu Etxezarreta Martinez, Patricio Fuentes, Pedro M Crespo, and Javier Garcia-Frias. Approximating decoherence processes for the design and simulation of quantum error correction codes on classical computers. *IEEE Access*, 8:172623–172643, 2020.
- [51] Shuaining Zhang, Yao Lu, Kuan Zhang, Wentao Chen, Ying Li, Jing-Ning Zhang, and Kihwan Kim. Error-mitigated quantum gates exceeding physical fidelities in a trapped-ion system. *Nature communications*, 11(1):587, 2020.
- [52] Ryan LaRose, Andrea Mari, Sarah Kaiser, Peter J Karalekas, Andre A Alves, Piotr Czarnik, Mohamed El Mandouh, Max H Gordon, Yousef Hindy, Aaron Robertson, et al. Mitiq: A software package for error mitigation on noisy quantum computers. *Quantum*, 6:774, 2022.
- [53] Ewout Van Den Berg, Zlatko K Mineev, Abhinav Kandala, and Kristan Temme. Probabilistic error cancellation with sparse pauli-lindblad models on noisy quantum processors. *Nature Physics*, pages 1–6, 2023.